1	Differential control of SK channel diffusion by actin in different neuronal
2	subcompartments
3	
4	Shiju Gu ¹ , Anastasios V. Tzingounis ^{1,2,3} , and George Lykotrafitis ^{1,3}
5	¹ Department of Biomedical Engineering, ² Department of Physiology and Neurobiology, and
6	³ Department of Mechanical Engineering, University of Connecticut, Storrs, CT 06269, USA
7	
8	
9 10 11 12 13 14	*Correspondence: George Lykotrafitis, PhD Department of Mechanical Engineering, University of Connecticut Storrs, CT 06269, USA Email: george.lykotrafitis@uconn.edu
15 16 17 18 19 20 21	Keywords: potassium channels, single particle tracking, axon initial segment, actin barrier crowding, cholesterol, spectrin network
23	
24	
25	
26	
27	
28 29	
30	
31	

Abstract

32

33

34

35

36

37

38

39

40

41

42

43

44

45

46

47

48

49

50

51

Small-conductance calcium-activated potassium (SK) channels show a ubiquitous distribution on neurons, in both somatodendritic and axonal regions. SK channels are associated with neuronal activity regulating action potential frequency, dendritic excitability, and synaptic plasticity. Although the physiology of SK channels and the mechanisms that control their surface expression levels have been investigated extensively, little is known about what controls SK channel diffusion in the neuronal plasma membrane. This aspect is important, as the diffusion of SK channels at the surface may control their localization and proximity to calcium channels, hence increasing the likelihood of SK channel activation by calcium. In this study, we successfully investigated the diffusion of SK channels labeled with quantum dots on human embryonic kidney cells and dissociated hippocampal neurons by combining a single-particle tracking method with total internal reflection fluorescence microscopy. We observed that actin filaments interfere with SK mobility, decreasing their diffusion coefficient. We also found that during neuronal maturation, SK channel diffusion was gradually inhibited on somatodendritic compartments. Importantly, we observed that axon barriers formed at approximately days in vitro (DIV) 6 and restricted the diffusion of SK channels on the axon initial segment (AIS). However, after neuron maturation, SK channels on the AIS were strongly immobilized, even after disruption of the actin network, suggesting that crowding may cause this effect. Altogether, our work provides insight into how SK channels diffuse on the neuronal plasma membrane and how actin and membrane crowding impacts SK channel diffusion.

53

52

Introduction

55

56

57

58

59

60

61

62

63

64

65

66

67

68

69

70

71

72

73

74

75

76

Small-conductance calcium-activated potassium (SK) channels are widely expressed in neurons across the nervous system. Their main function is to prevent excessive neuronal depolarization in response to calcium influx following neuronal activity. SK channels typically activate in spines and dendrites, preventing sustained dendritic depolarization. Consequently, loss of SK channel activity leads to prolonged calcium signals in dendrites and elevated N-methyl-D-aspartate (NMDA) receptor activity in synapses. Besides dendrites, SK channels are also expressed in the soma and, to a lesser extent, in axons. The somato-axonal location of SK channels is likely responsible for their contribution to medium afterhyperpolarization (mAHP) and spike frequency adaptation. The mAHP a brief quiescence period (100-200 ms) following a bout of action potentials. Thus, it is not surprising that SK channels have emerged as key regulators for learning and memory, sleep, and neuronal computations in general. Because of the strong ability of SK channels to control neuronal activity, their properties and levels are highly regulated in neurons. These regulated properties include surface expression and clustering in the plasma membrane. For instance, we and others have demonstrated that the surface expression of SK channels is limited by the cyclic adenosine monophosphate-protein kinase A (cAMP-PKA) signaling pathway ¹⁻⁴. Besides intracellular signaling cascades, SK channels are also tethered to the actin cytoskeleton through a-actinin and filamin A, providing another means of regulation 5-7. Although several studies have focused on the physiology of SK channels and the mechanisms that control their surface levels, little is known about what controls SK channel diffusion in the plasma membrane and different neuronal compartments. This aspect is particularly important, as the diffusion of SK channels at the surface could control their density. Increased SK

channel clustering in proximity to calcium sources would allow for increased likelihood of SK channel activation by calcium.

A key advance over the last ten years has been the recognition that different neuronal compartments have substantially different actin–spectrin cytoskeleton geometries, which, in some cases, can dictate the diffusion of membrane proteins and lipids. For instance, super-resolution microscopy has shown that the actin cytoskeleton of neuronal axons exhibits a periodic structure consisting of azimuthal actin rings with a periodicity of 180~190 nm. These actin rings are connected via longitudinal spectrin tetramers ⁸. Previous work has also shown that this axon membrane periodic skeleton interferes with the diffusion of lipids, integral monotopic proteins of the inner leaflet, and, more significantly, transmembrane proteins ⁹. Specifically, glycosylphosphatidylinositol-anchored green fluorescent protein (GPI-GFP) molecules exhibit an approximately 190-nm periodic striped pattern spaced by adjacent actin rings in axons ¹⁰. Actin filaments in the dendrites are also expected to affect ion channel diffusion, as previously shown for α-amino-3-hydroxy-5-methyl-4-isoxazole (AMPA) receptors ¹¹. In contrast to axons and dendrites, the actin–spectrin cytoskeleton follows a different two-dimensional (2D) arrangement in the soma, more akin to previous observations in red blood cells.

In this work, we sought to investigate SK channel diffusion in the soma, dendrites, and axons of pyramidal hippocampal neurons at different maturation stages. To achieve this goal, we used apamin, a bee venom that specifically blocks SK channels ^{4,12-14}, conjugated with quantum dots (QDs). This approach allowed us to successfully track and analyze the diffusion of individual native SK channels on cultured hippocampal neurons.

Methods

99

Reagents: We purchased KT5720 (K3761), Latrunculin B (LatB; L5288), Rp-cAMP 100 triethylammonium salt (Rp-cAMPS; A165), methyl-β-cyclodextrin-cholesterol (MβCD-101 102 cholesterol; C4951), filipin complex (F9765) from MilliporeSigma (St. Louis, MO). Swinholide A (SwinA) was purchased from Cayman Chemical Company (19611; Ann Arbor, MI) and 103 104 Cytochalasin D (CytoD) was purchased from Thermo Fisher Scientific (PHZ1063; Waltham, MA). We obtained XE991 from Tocris Bioscience (2000; Bristol, UK). Apamin-biotin was obtained 105 from Alomone Labs (STA-200-B; Jerusalem, Israel). 106 **Neuron cultures:** We first treated embryonic day 18 rat hippocampal tissues purchased from 107 BrainBits (SDEHPS; Springfield, IL) with trypsin (15400054; Thermo Fisher Scientific) and then 108 109 placed the tissue on poly-D-lysine-coated (P0899; MilliporeSigma, Burlington, MA) glass-bottom petri dishes (14027-20; Ted Pella, Inc., Redding, CA) and coverslips (12-545-83; Fisher Scientific 110 International, Inc., Hampton, NH) at a density of 150,000 cells/dish and 75,000 cells/coverslip, 111 respectively. We cultured all neurons in neurobasal medium supplied with B27 supplement, 112 penicillin streptomycin, and GlutaMAX. These solutions were all purchased from Thermo Fisher 113 Scientific. We maintained the neurons in a 37°C humidified incubator with 5% CO₂ ¹⁵. 114 Transfection of human embryonic kidney (HEK) cells: HEK293T cells were split every 3 days 115 and maintained in Dulbecco's Modified Eagle's Medium (DMEM) supplemented with 10% fetal 116 117 bovine serum, sodium pyruvate, and penicillin streptomycin (Thermo Fisher Scientific). One day prior to transfection, we placed the HEK293T cells on glass-bottom petri dishes at a density of 118 850,000 cells/dish. After approximately 24 h, we transfected the cells with 1.5 µg SK2-L plasmid 119 120 by using Lipofectamine 3000 transfection reagent (Thermo Fisher Scientific) according to the manufacturer's instructions. All experiments were conducted 36–48 h after transfection. 121

124

125

126

127

128

129

130

131

132

133

134

135

136

137

138

139

140

141

142

143

144

Immunocytochemistry: To stain the axon initial segment (AIS) in live neuron experiments, we applied 2 µg/mL anti-pan-neurofascin antibody (75-112; Antibodies Incorporated, Davis, CA) for 3 min at room temperature (RT). After rinsing three times, we blocked the neurons with 1% bovine serum albumin (BSA; A7030; MilliporeSigma) for 3 min at RT. Next, we incubated neurons with goat anti-mouse Alexa Fluor 568 conjugate (1:500; RRID: AB 2534072; Thermo Fisher Scientific; also contains 1% BSA) for 2 min at RT. The neurons were then rinsed six times and returned to the incubator for 3 min prior to the subsequent experiments. We visualized the AIS by applying a 561-nm diode laser to excite Alexa Fluor 568 at 1% laser intensity. All washing and incubation steps mentioned above were conducted with Tyrode's solution consisting of Tyrode's Salts (T2145; MilliporeSigma), 10 mM HEPES (15630080; Thermo Fisher Scientific), and 3.5 mM sucrose (S9378; MilliporeSigma), pH7.4, 305–310 mOsm ¹⁶. Cholesterol modulation: DIV4 neurons were treated with MβCD-cholesterol solution in DI water at a final concentration of 1.5mM, 3mM or 5mM at 37°C for 0.5 h. The neurons were rinsed three times and fixed with 4% paraformaldehyde (15710; Electron Microscopy Sciences; Hatfield; PA) for 15 minutes at RT. After washing three times with dPBS (14190144; Themo Fisher Scientific), 50mM NH4CL (A9434; MilliporeSigma) solution was added for 10 min to quench the autofluorescence. Neuron were washed three times with dPBS and blocked with preblock buffer (5% normal goat serum in PBS) for 0.5 h. Anti-pan-neuronfascin antibody were then added to neurons at a final concentration of 2 µg/mL in preblock buffer for 2 h at RT, followed by three rinses with preblock buffer. Neurons were next incubated with 40 µM filipin (F9765; MilliporeSigma) to stain cholesterol and goat anti-mouse Alexa Fluor 568 conjugate (1:500) to stain NF186 antibody, which specifically labels the AIS, for 2 h at RT in the dark. After washing

six times with dPBS, neurons were mounted on glass slides using Prolong Diamond Antifade Mountant (P36965; Thermo Fisher Scientific).

Fluorescent images were collected via a laser-scanning Leica SP8 (Leica Microsystems, Wetzlar, Germany) confocal microscope using LAS X software. 405-nm laser was used to excite filipin at 2% laser intensity and 561-nm laser was used to excite Alexa Fluor 568 conjugate at 4% laser intensity. Z-stack images were collected and we applied maximum intensity projection. We next measured the fluorescent intensity of filipin in ImageJ (NIH, Bethesda, MD) software. To obtain the corrected total fluorescence (CTF) ratio, we first calculated the average background fluorescence by randomly selecting three areas of $15 \, \mu m^2$ and then we measured their mean intensity value. To obtain the CTF at a location on a neuron, we measured the mean signal intensity of the corresponding area and then we applied the equation CTF = mean signal intensity – mean background intensity. Finally, we repeated this measurement at different locations (30 for AIS and soma, 60 for dendrites). Each CTF value was divided by the mean value of a control group without cholesterol uptake at the same imaging conditions to derive the CTF ratio.

QD labeling: The first reagent (1 μM KT5720, 10 μM Rp-cAMPS, or 0.1% (v/v) dimethylsulfoxide [DMSO] carrier) was added to a petri dish and incubated for 0.5 h, followed by a 0.5-h incubation of the second reagent [125 nM SwinA, 10 μM LatB, 5 μM CytoD or 2 μL DMSO carrier]. We briefly washed the dish and then added apamin-biotin (10 nM) for 3 min at RT. After rinsing the petri dish three times, we blocked the cells with 1% BSA for 3 min at RT. Next, we added 0.3 nM Qdot 655 streptavidin conjugate (Q10123MP; Thermo Fisher Scientific; also contains 1% BSA) for 2 min at RT. BSA minimizes nonspecific binding between QDs and the dish substrate, while the low QD concentration allows us to track single dots. The concentration and timing of QD application listed above were empirically determined. Finally, we rinsed the

cells six times and returned the cells to the incubator for 3 min prior to the subsequent experiments.

All washing and incubation steps mentioned above were conducted with Tyrode's solution.

Single-particle tracking (SPT) using total internal reflection fluorescence (TIRF) microscopy:

For recording, we utilized an inverted stand Nikon Eclipse TiE microscope equipped with an Andor iXon back-illuminated frame transfer electron-multiplying charge-coupled device (EMCCD) camera. To image the QD locations, we applied a 100X oil immersion lens with a numerical aperture of 1.49. The QDs were excited by a 405-nm diode laser. During imaging, the temperature was maintained at 37° C by an Okolab cage incubator and a Pathology Devices LiveCell stage top incubator. We used Micro-Manager software to operate the microscope and recorded movies at a rate of 9 frames/s with an exposure time of 100 ms. We recorded at least 900 frames (100 s) for each movie, with a pixel size of $0.11 \times 0.11 \,\mu m$.

Image processing and analysis: Movie tracking and processing were conducted via u-track software ¹⁷ and MATLAB. After initial processing with u-track, we removed low-illumination signals and out-of-focus dots. Then, we utilized the coordinates of QDs in each frame of the image series, which were acquired by u-track, as an input to an in-house-developed MATLAB code to calculate the time-averaged mean square displacement (TA-MSD) by employing the following equation:

$$\overline{\delta^2(t_{lag})} = \frac{1}{T - t_{lag}} \int_0^{T - t_{lag}} \left| r(t + t_{lag}) - r(t) \right|^2 dt$$

Here, $\overline{\delta^2(t_{lag})}$ is the TA-MSD, t_{lag} is the lag time (time between adjacent frames), T is the total time of the movie, and r(t) is the 2D position of the SK channel at time t.

After obtaining the TA-MSD, we calculated the diffusion coefficient using the following equation:

 $\overline{\delta^2(t_{lag})} = 4Dt_{lag}$

where D is the diffusion coefficient of the SK channel.

Statistical analysis: The results related to diffusion coefficients were analyzed and reported using

192 GraphPad Prism (GraphPad Software, Inc., San Diego, CA). We performed nonparametric Mann-

Whitney tests to compare results. Results were considered significant for P < 0.05. *P < 0.05,

P < 0.01, *P < 0.001; n.s. indicates no significant difference.

195

196

197

198

199

200

201

191

193

194

Results

We attached QDs to SK channels by incubating cells in apamin-biotin followed by a streptavidin—QD conjugate. Biotin forms a strong bond with streptavidin, allowing us to monitor SK channel diffusion by tracking QDs using the SPT method. Fig. 1 illustrates typical trajectories of QDs conjugated to SK channels. The trajectories are superimposed on the soma, dendrites, and the AIS of a representative neuron.

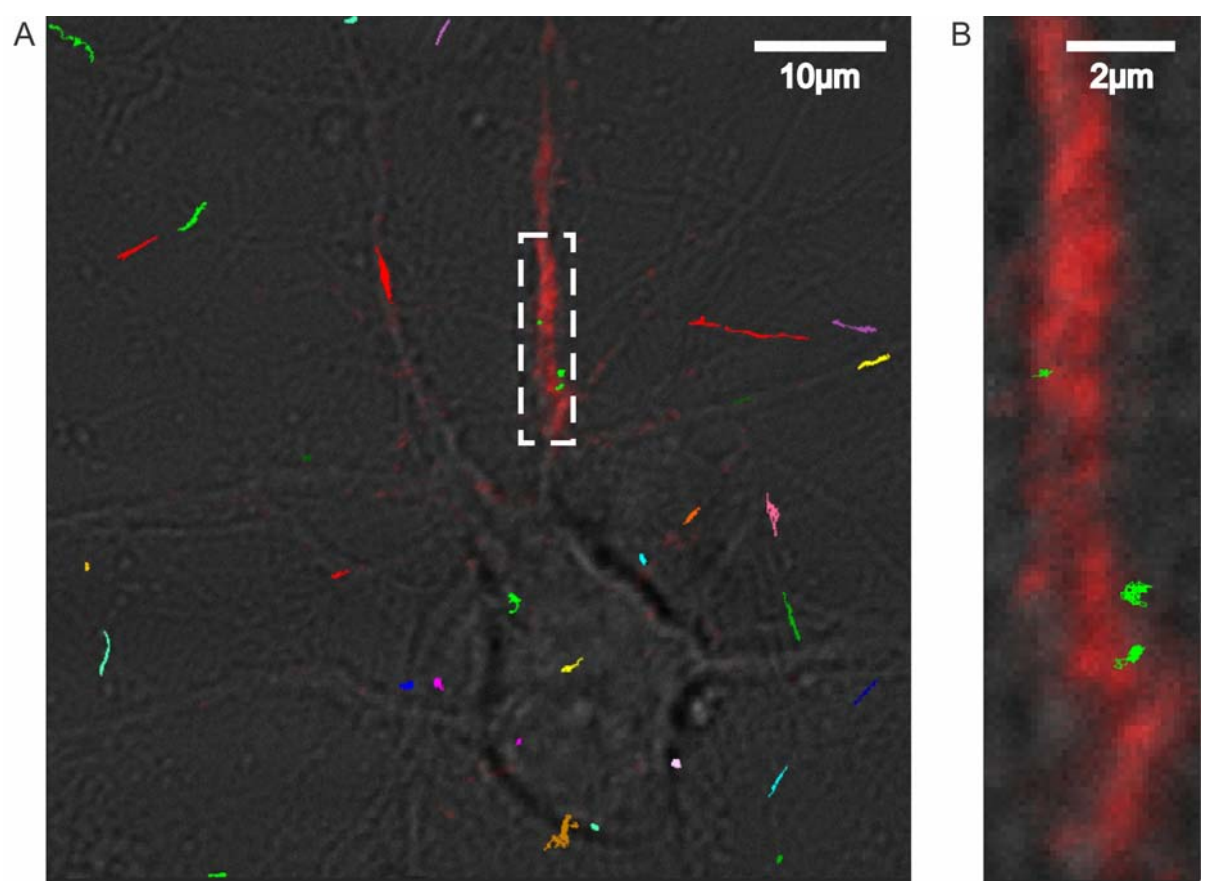


Fig. 1. (A) Typical trajectories of QDs attached to diffusing SK channels superimposed on the corresponding neuron. (B) Magnified view of the boxed area in panel A indicating part of the AIS in red.

SK channel diffusion in HEK293T cells

203

204

205

206

207

208

209

210

211

212

213

214

215

216

217

218

219

220

221

222

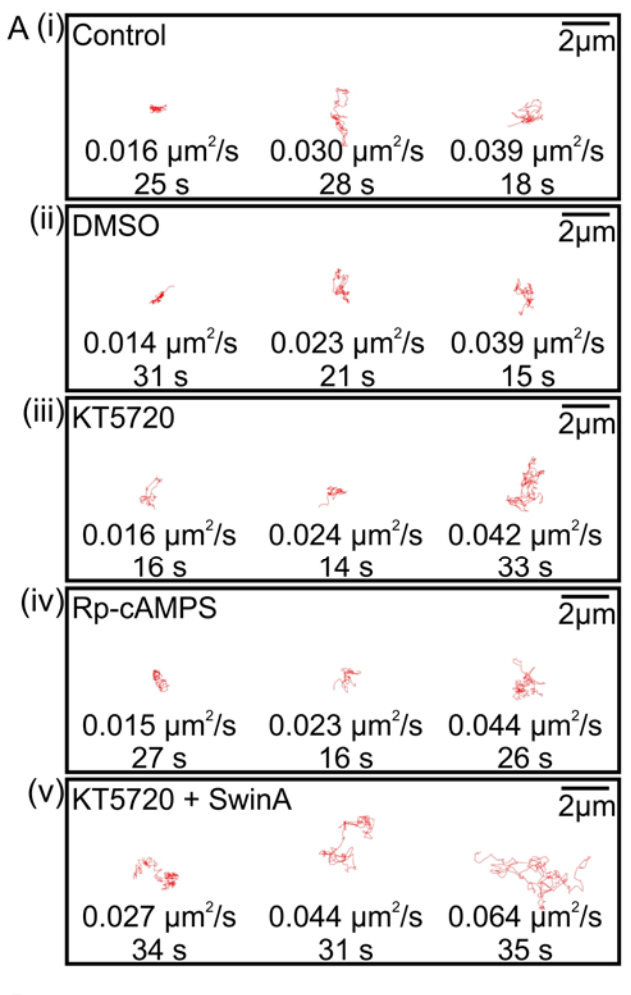
223

224

225

We performed experiments on HEK293T cells to test the specificity of our apamin-conjugated QDs. For this, we compared cells transfected with SK2 type channels, which is the most common subtype of SK channels, and untransfected cells from sister cultures. To increase the number of SK2 channels at the cell surface, we pretreated our cells with KT5720, a PKA inhibitor. We and others have shown that ongoing PKA activity controls SK2 cell surface expression ^{1,2,4,15,18,19}. We sequentially treated both groups of cells with KT5720, DMSO, apamin-biotin, and streptavidinconjugated QDs (see Methods). Consistent with the apamin–QD specificity, we found a significant difference between the number of QDs on transfected cells and those on non-transfected cells in a $60 \times 60 \,\mu m$ area (Fig. S1). This result indicates that the large majority of QDs detected on transfected HEK293T cells were specifically bound to SK2 channels. Next, we examined SK2 channel diffusion in HEK293T cells and its dependency on ongoing PKA activity and the actin cytoskeleton. We expected these results to provide a benchmark for SK2 diffusion in cells with a 2D lattice actin-spectrin cytoskeleton. Because all drugs, including KT5720, were dissolved in DMSO, we first assessed whether DMSO alone affects SK2 channel diffusion on HEK293T cells. At 36–48 h following transfection with SK2 plasmids, one group of cells was left untreated, serving as the control group, whereas another group of cells was incubated with DMSO for 1 h. We first plotted representative trajectories of QDs for both conditions [Fig. 2A(i), 2A(ii)]. We calculated the diffusion coefficient for both groups and performed a nonparametric Mann-Whitney test, which showed no significant difference between these two groups (Fig. 2B; control: $D = 0.022 \pm 0.013 \,\mu m^2 / s$; DMSO: $D = 0.021 \pm 0.012 \,\mu m^2 / s$, P = 0.7500). This result indicates that DMSO alone does not affect SK channel diffusion. Next, we assessed whether KT5720 interferes with SK channel diffusion and compared the results to

- 226 those for the control group. We observed that the particle trajectories in the two cases are similar
- 227 [Fig. 2A(iii)], with no significant difference between the two diffusion coefficients (Fig. 2B;
- 228 KT5720: $D = 0.024 \pm 0.012 \,\mu m^2 / s$, P = 0.5085).
- To confirm that inhibiting PKA does not affect SK channel diffusion, we also used Rp-cAMPS,
- 230 which is a competitive cAMP analog that inhibits cAMP-induced activation of PKA ¹⁵. Similar to
- 231 KT5720, Rp-cAMPS increases SK2 channel expression. As with our KT5720 experiments, we
- found that Rp-cAMPS did not significantly influence SK channel diffusion, as shown by the QD
- trajectories [Fig. 2A(iv)] and diffusion coefficient (Fig. 2B; Rp-cAMPS: $D = 0.021 \pm 0.021$
- $0.012 \,\mu m^2 / s$, P = 0.8486). These findings demonstrate that SK channel diffusion in the
- HEK293T plasma membrane was not affected by DMSO, KT5720, or Rp-cAMPS.
- Recently, it has been recognized that the actin cytoskeleton can regulate the trafficking and
- 237 diffusion of membrane proteins ²⁰⁻²². Considering that SK2 channels interact with the actin
- 238 cytoskeleton though a-actinin2 and filamin A 5-7, we examined whether disruption of the actin
- 239 cytoskeleton alters SK2 channel diffusion. We used SwinA, a toxin that disrupts the actin
- 240 cytoskeleton by both sequestering G-actin and severing F-actin ²³. We applied SwinA to HEK293T
- cells for 30 min, based on the protocol reported in ²⁴. We found that SK2 channels in SwinA-
- treated cells were more mobile and their trajectories covered a greater area in the same time frame
- 243 [Fig. 2A(v)]. This led to a significant increase in their diffusion coefficient (Fig. 2B; KT5720 +
- SwinA: $D = 0.032 \pm 0.013 \,\mu m^2 / s$, P = 0.017). This result, compared with the KT5720,
- suggests that the actin-based skeleton regulates SK channel diffusive motion since addition of
- 246 SwinA degrades the actin skeletal filaments ²³.



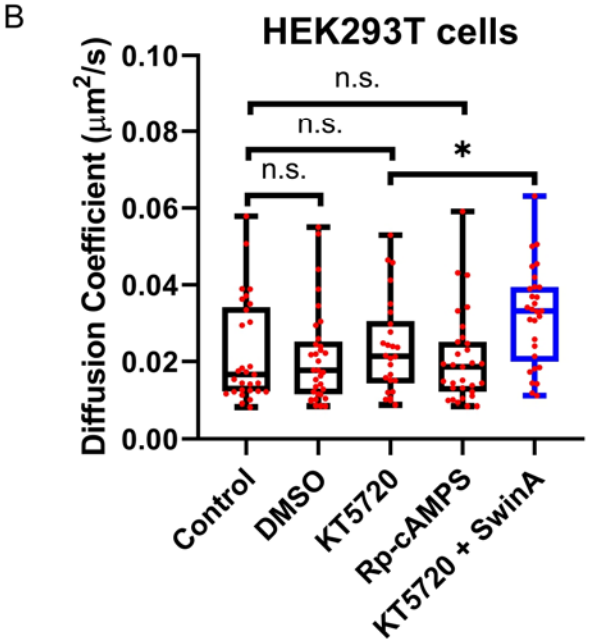


Fig. 2. Diffusion of SK channels in **HEK293T** transfected cells. (A) Representative diffusion trajectories of SK channels in transfected HEK293T cells labeled with 10 nM apamin-biotin and 0.3 nM streptavidin-QDs after preincubation with: (i) no reagent, (ii) DMSO for 30 min, (iii) 1 µM KT5720 for 30 min, (iv) 10 µM Rp-cAMPS for 30 min, or (v) 1 µM KT5720 for 30 min and then 125 nM SwinA for 30 min. (B) Box and whisker plots showing the diffusion coefficients of SK channels in transfected HEK293T cells under different conditions (control: $D = 0.022 \pm 0.013 \,\mu m^2 / s$, n =29; DMSO: $D = 0.021 \pm 0.012 \,\mu m^2 / s$, n = 33; KT5720: $D = 0.024 \pm 0.012 \,\mu m^2$ s , n = 26 ; Rp-cAMPS: $D = 0.021 \pm 0.021$ $0.012 \,\mu m^2 / s$, n = 31; KT5720 + SwinA: $D = 0.032 \pm 0.013 \,\mu m^2 / s$, n = 29). n.s., no significant difference. * P < 0.05 (Mann– Whitney test).

Diffusion of SK channels in neurons

271

272

273

274

275

276

277

278

279

280

281

282

283

284

285

286

287

288

289

290

291

292

293

to which SK channel diffusion differs in various neuronal subcompartments, we used a similar approach as with our HEK293T measurements. First, we confirmed the specificity of apaminbiotin-streptavidin-QD conjugate to SK channels in neurons. To distinguish an axon from dendrites in live neurons, we visualized the AIS by combining neurofascin-186 (NF186) antibody with Alexa Fluor 568, as research indicates that NF186 is highly enriched at the AIS ¹⁰. We treated neurons at DIV18 with KT5720 followed by DMSO. As with our HEK293T experiments, application of KT5720 increased SK cell surface expression and the signal-to-noise ratio. Next, we simultaneously added the NF186 antibody and apamin-biotin conjugates, followed by streptavidin QDs and Alexa Fluor 568. In another set of neurons, we repeated the aforementioned procedures while emitting apamin-biotin from the media. In four $60 \times 60 \,\mu m$ areas, the number of detected QDs was significantly less in the absence of apamin-biotin (Fig. S2). This result demonstrates that our OD conjugate has a high binding specificity. Next, we assessed the effects of KT5720 and SwinA on the diffusion of SK channels in different neuronal subcompartments and at different developmental time points. We first focused on neurons cultured for DIV10, a time point at which we could detect the diffusion of SK channels in all neuronal subcompartments. By contrast, in more mature neurons, the diffusion of SK channels was selective depending on the specific subcompartment, and in less mature neurons, we could detect diffusion in all subcompartments but without large variations in the diffusion coefficients as seen at DIV10. As with our prior results, DMSO did not alter SK channel diffusion in neurons. Indeed, we found no significance differences in the SK channel diffusion coefficients between the control and DMSO samples in somas (Fig. 3A; control: $D = 0.025 \pm 0.019 \,\mu m^2 / s$; DMSO:

To test the diffusion of SK channels in neurons under different conditions and determine the extent

- 294 $D = 0.024 \pm 0.020 \,\mu\text{m}^2 / \text{s}$, P = 0.9273), dendrites (Fig. 3B; control: $D = 0.034 \pm$
- 295 0.021 $\mu m^2 / s$; DMSO: $D = 0.034 \pm 0.018 \,\mu m^2 / s$, P = 0.9786), or the AIS (Fig. 3C; control:
- 296 $D = 0.002 \pm 0.001 \,\mu m^2 / s$; DMSO: $D = 0.003 \pm 0.002 \,\mu m^2 / s$, P = 0.6857).
- We also investigated whether KT5720 affects the diffusion of SK channels in neurons. Our results
- show that applying KT5720 did not cause a significant difference in the diffusion coefficient of
- 299 SK channels in somas when compared with the control group (Fig. 3A; KT5720: $D = 0.019 \pm 0.019$
- $0.016 \,\mu\text{m}^2 \,/\,\text{s}$, P = 0.5918). Likewise, we detected no significant differences in dendrites (Fig.
- 301 3B; KT5720: $D = 0.034 \pm 0.019 \,\mu m^2 / s$, P = 0.9031) or the AIS (Fig. 3C; KT5720: D =
- $0.004 \pm 0.002 \,\mu m^2 / s$, P = 0.2828). In addition to DIV10, we also confirmed that KT5720 did
- not have a significant effect on the diffusion coefficient of SK channels in neurons at DIV14 and
- 304 DIV18 (Fig. S3).
- However, after applying SwinA, we detected significant increases in the diffusion coefficients of
- 306 SK channels in somas (Fig. 3A; KT5720 + SwinA: $D = 0.031 \pm 0.012 \,\mu m^2 / s$, P = 0.0148)
- and dendrites (Fig. 3B; KT5720 + SwinA: $D = 0.040 \pm 0.019 \,\mu\text{m}^2 / \text{s}$, P = 0.0347) in
- 308 comparison with the KT5720 group. After treating neurons with SwinA, we also observed an
- elevated mobility of QDs at the AIS (Fig. 3C; KT5720 + SwinA: $D = 0.015 \pm 0.010 \,\mu m^2 / s$,
- 310 P = 0.0281). To determine whether actin polymerization inhibition or severing actin was
- 311 responsible for the observed SK diffusion variations, we repeated our experiments using LatB, a
- compound that inhibits the polymerization of actin filaments ²⁵. We found that, compared with the
- 313 KT5720 group, treating neurons with LatB did not cause any significant differences in the
- diffusion coefficient of SK channels in somas (Fig. 3A; KT5720 + LatB: $D = 0.031 \pm$
- 315 $0.025 \,\mu m^2 / s$, P = 0.3431), dendrites (Fig. 3B; KT5720 + LatB: $D = 0.036 \pm 0.025 \,\mu m^2 / s$,
- 316 P = 0.8950), or the AIS (Fig. 3C; KT5720 + LatB: $D = 0.004 \pm 0.002 \,\mu m^2 / s$, P > 0.9999).

This finding likely reflects the lower potency of LatB compared with SwinA, as LatB only inhibits the polymerization of actin while SwinA also severs the existing actin filaments 23,26 . To further confirm that actin network disorganization results in an increase of SK channel diffusion coefficient we treated neurons with CytoD, a compound that leads to widespread disruption of the actin network through multiple mechanisms, $^{27-29}$. Indeed, we observed a significant increase in the diffusion coefficient of SK channels in somas (Fig. 3A; KT5720 + CytoD: $D = 0.031 \pm 0.015 \,\mu m^2 / s$, P = 0.0345), dendrites (Fig. 3B; KT5720 + CytoD: $D = 0.040 \pm 0.018 \,\mu m^2 / s$, P = 0.0428), and the AIS (Fig. 3C; KT5720 + CytoD: $D = 0.023 \pm 0.021 \,\mu m^2 / s$, P = 0.0401) compared to the corresponding controls. In summary, CytoD shows an effect similar to SwinA and stronger than LatB. This result agrees with the observation that the periodic actin rings in the AIS are relatively stable to treatment with Latrunculins A and B 30,31 .

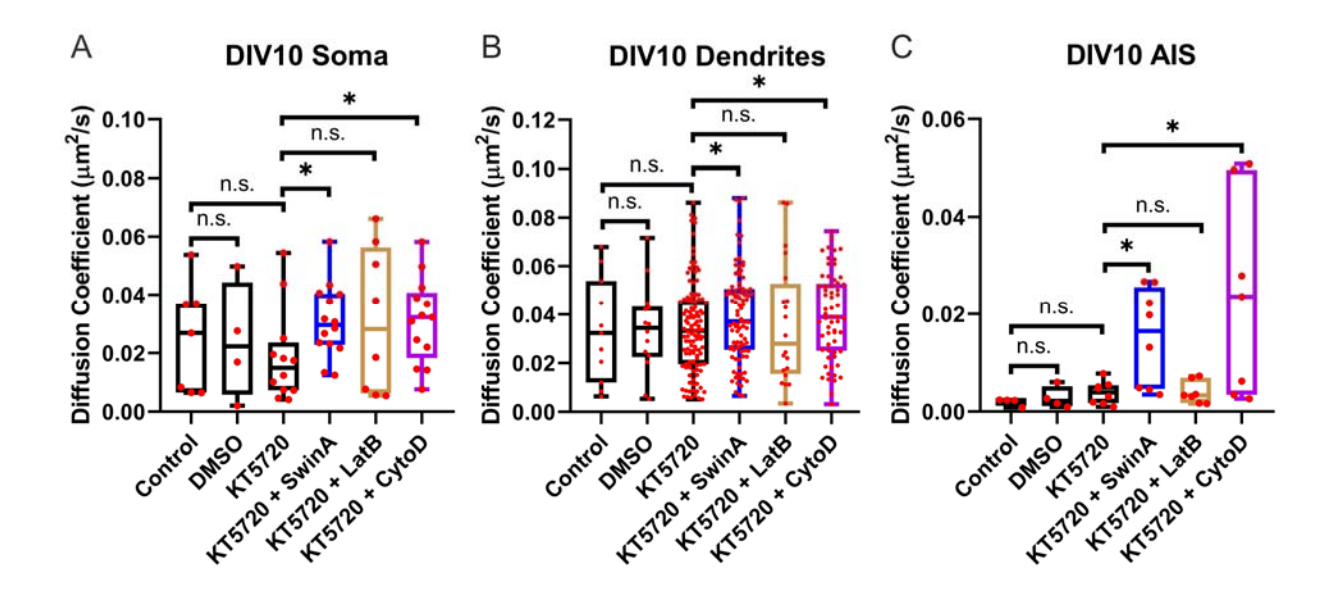


Fig. 3. Diffusion of SK channels in hippocampal neurons at DIV10. Box and whisker plots showing the diffusion coefficients of SK channels in the plasma membranes of various compartments of dissociated hippocampal neurons at DIV10 following different treatments: (A) soma (control: $D = 0.025 \pm 0.019 \,\mu m^2 / s$, n = 7; DMSO: $D = 0.024 \pm 0.020 \,\mu m^2 / s$, n = 7

- 333 4 ; KT5720: $D = 0.019 \pm 0.016 \,\mu m^2 / s$, n = 12 ; KT5720 + SwinA: $D = 0.031 \pm 0.016 \,\mu m^2 / s$
- 334 $0.012 \,\mu m^2 / s$, n = 14; KT5720 + LatB: $D = 0.031 \pm 0.025 \,\mu m^2 / s$, n = 8; KT5720 +
- 335 CytoD: $D = 0.031 \pm 0.015 \,\mu m^2 / s$, n = 13), (B) dendrites (control: $D = 0.034 \pm 0.015 \,\mu m^2 / s$)
- 336 $0.021 \,\mu m^2 / s, n = 11$; DMSO: $D = 0.034 \pm 0.018 \,\mu m^2 / s, n = 14$; KT5720: $D = 0.034 \pm 0.018 \,\mu m^2 / s$
- 337 $0.019 \,\mu m^2 / s$, n = 121; KT5720 + SwinA: $D = 0.040 \pm 0.019 \,\mu m^2 / s$, n = 96; KT5720 +
- 338 LatB: $D = 0.036 \pm 0.025 \,\mu m^2 / s$, n = 20; KT5720 + CytoD: $D = 0.040 \pm 0.018 \,\mu m^2 / s$,
- 339 n = 61), and (C) AIS (control: $D = 0.002 \pm 0.001 \,\mu m^2 / s$, n = 4; DMSO: $D = 0.003 \pm 0.001 \,\mu m^2 / s$
- 340 $0.002 \,\mu m^2 / s$, n = 4; KT5720: $D = 0.004 \pm 0.002 \,\mu m^2 / s$, n = 8; KT5720 + SwinA: $D = 0.002 \,\mu m^2 / s$
- 341 $0.015 \pm 0.010 \,\mu m^2 / s$, n = 8; KT5720 + LatB: $D = 0.004 \pm 0.002 \,\mu m^2 / s$, n =
- 342 7; KT5720 + CytoD: $D = 0.023 \pm 0.021 \,\mu m^2 / s, n = 7$). n.s., no significant difference. *
- 343 P < 0.05 (Mann–Whitney test).

- Neuronal maturation is accompanied by an increase in membrane crowding as well as maturation
- of the actin cytoskeleton, suggesting that SK channel diffusion might also be altered accordingly.
- To address this possibility, we performed experiments at different maturation points: DIV4, 6, 10,
- 348 14, and 18. We treated all neurons with KT5720 in DMSO, and then treated one group of neurons
- with SwinA in DMSO and the control group with only DMSO.
- In soma, at DIV4 and 6, application of SwinA led to a non-significant increase in the diffusion
- coefficient of SK channels [Fig. 4A(i), A(ii), B; DIV4 (KT5720): $D = 0.039 \pm 0.013 \,\mu m^2 / s$;
- 352 DIV4 (KT5720 + SwinA): $D = 0.050 \pm 0.015 \,\mu m^2 / s$, P = 0.0800; Fig. 4A(iii), A(iv), B;
- 353 DIV6 (KT5720): $D = 0.034 \pm 0.014 \,\mu m^2 / s$; DIV6 (KT5720 + SwinA): $D = 0.039 \pm 0.014 \,\mu m^2 / s$
- $0.018 \,\mu m^2 / s$, P = 0.4463]. In contrast, we found that as neurons matured, the SK diffusion

coefficient significantly increased between the SwinA-treated and control groups. For instance, at DIV10, SK channel diffusion increased in the soma following disruption of the actin cytoskeleton lattice [Fig. 4A(v), A(vi), B; DIV10 (KT5720): $D = 0.019 \pm 0.016 \,\mu m^2 / s$; DIV10 (KT5720 + SwinA): $D = 0.031 \pm 0.012 \,\mu m^2 / s$, P = 0.0148]. Similar results emerged for neurons at DIV14 and 18 [Fig. 4A(vii), A(viii), B; DIV14 (KT5720): $D = 0.015 \pm 0.010 \,\mu m^2 / s$; DIV14 (KT5720 + SwinA): $D = 0.029 \pm 0.010 \,\mu\text{m}^2 / \text{s}$, P = 0.0380; Fig. 4A(ix), A(x), B; DIV18 (KT5720): $D = 0.009 \pm 0.008 \,\mu m^2 / s$; DIV18 (KT5720 + SwinA): $D = 0.026 \pm 0.017 \,\mu m^2 / s$ s, P = 0.0176]. We also note that there is a significant diffusion coefficient linear trend decrease (P < 0.01) for both the control and the SwinA-treated groups during the initial cell maturation period from DIV4 to DIV10. However, the diffusion coefficient remained stable during the latest period of neuron maturation from DIV10 to DIV18. Based on the results above, we can conclude that as neurons develop and they gradually establish an actin-based plasma membrane somatic cytoskeleton with a polygonal lattice structure ³², the diffusion of SK channels is affected. At early stages of maturity, the formation of the actin-based membrane skeleton is still in progress and, thus, it causes a significant gradual decrease in the diffusion coefficient of SK channels. It appears that after DIV10 the network was fully developed or further development had a minimal additional effect on SK channel diffusion. We also observed that the effect of SwinA is significant in the latest stages of neuronal maturation (DIV10 to DIV18) since disruption of a well-formed membrane skeleton had a more significant effect on diffusion than disruption of a membrane skeleton earlier in neuronal development (DIV4 and 6).

355

356

357

358

359

360

361

362

363

364

365

366

367

368

369

370

371

372

373

374

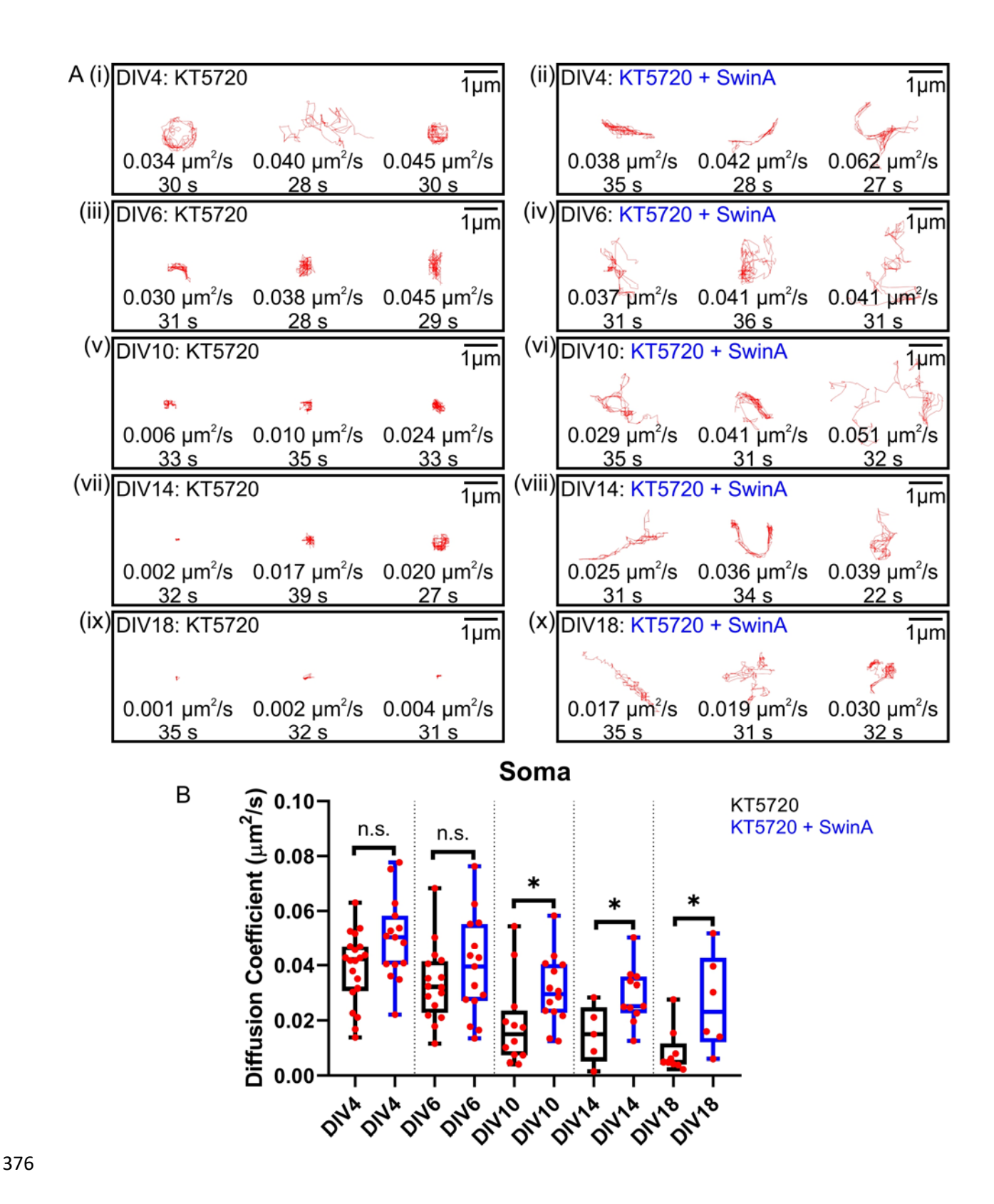


Fig. 4. Diffusion of SK channels in the plasma membranes of somas. (A) Representative diffusion trajectories of SK channels in the plasma membranes of the somas of hippocampal

neurons at various developmental time points after a 30-min preincubation with 1 µM KT5720 or 379 1 μM KT5720 followed by a 30-min incubation with 125 nM SwinA. (B) Box and whisker plots 380 showing the diffusion coefficients of SK channels on soma under different conditions at various 381 developmental time points: DIV4 (KT5720: $D = 0.039 \pm 0.013 \,\mu m^2 / s$, n = 20; KT5720 + 382 Swin A: $D = 0.050 \pm 0.015 \,\mu m^2 \,/\, s$, n = 15), DIV6 (KT5720: $D = 0.034 \pm 0.014 \,\mu m^2 \,/\, s$, 383 n = 16; KT5720 + SwinA: $D = 0.039 \pm 0.018 \,\mu m^2 / s$, n = 15), DIV10 (KT5720: D =384 $0.019 \pm 0.016 \,\mu m^2 / s$, n = 12; KT5720 + SwinA: $D = 0.031 \pm 0.012 \,\mu m^2 / s$, n = 14), 385 DIV14 (KT5720: $D = 0.015 \pm 0.010 \,\mu m^2 / s$, n = 5; KT5720 + SwinA: $D = 0.029 \pm 0.010 \,\mu m^2$ 386 $0.010 \ \mu m^2 \ / \ s, \ n = 14), \ {\rm and \ DIV18} \ ({\rm KT5720}: D = 0.009 \pm 0.008 \ \mu m^2 \ / \ s, \ n = 9 \ ; \ {\rm KT5720} +$ 387 SwinA: $D = 0.026 \pm 0.017 \,\mu m^2 / s$, n = 6). n.s., no significant difference. * P < 0.05 (Mann– 388 389 Whitney test).

390

391 We also investigated the diffusion of SK channels in dendrites. Similar to the results for the soma, no significant differences in the SK channel diffusion coefficient emerged between control and 392 SwinA-treated neurons at DIV4 [Fig. 5A(i), A(ii), B; DIV4 (KT5720): $D = 0.048 \pm 0.019 \,\mu m^2$ 393 s; DIV4 (KT5720 + SwinA): $D = 0.053 \pm 0.020 \,\mu m^2 / s$, P = 0.3769] or at DIV6 [Fig. 5A(iii), 394 A(iv), B; DIV6 (KT5720): $D = 0.046 \pm 0.016 \,\mu m^2 / s$; DIV6 (KT5720 + SwinA): $D = 0.051 \pm 0.016 \,\mu m^2 / s$; DIV6 (KT5720 + SwinA): $D = 0.051 \pm 0.016 \,\mu m^2 / s$; 395 $0.015 \,\mu m^2 / s$, P = 0.2374]. However, application of SwinA led to a significant increase in the 396 SK channel diffusion coefficient compared with the control group at DIV10 [Fig. 5A(v), A(vi), B; 397 DIV10 (KT5720): $D = 0.034 \pm 0.019 \,\mu m^2 / s$; DIV10 (KT5720 + SwinA): $D = 0.040 \pm 0.019 \,\mu m^2 / s$ 398 $0.019 \,\mu m^2 / s$, P = 0.0135] and DIV14 [Fig. 5A(vii), A(viii), B; DIV14 (KT5720): D =399 $0.031 \pm 0.016 \,\mu m^2 / s$; DIV14 (KT5720 + SwinA): $D = 0.038 \pm 0.017 \,\mu m^2 / s$, P = 0.0100], 400 and an even larger increase at DIV18 [Fig. 5A(ix), A(x), B; DIV18 (KT5720): $D = 0.027 \pm 0.027$ 401

 $0.018 \,\mu m^2 / s$; DIV18 (KT5720 + SwinA): $D = 0.035 \pm 0.019 \,\mu m^2 / s$, P = 0.0006]. Taken together, our results suggest that containment of the diffusion of SK channels from actin-based membrane skeletons in dendrites becomes increasingly prominent during the development of neurons.

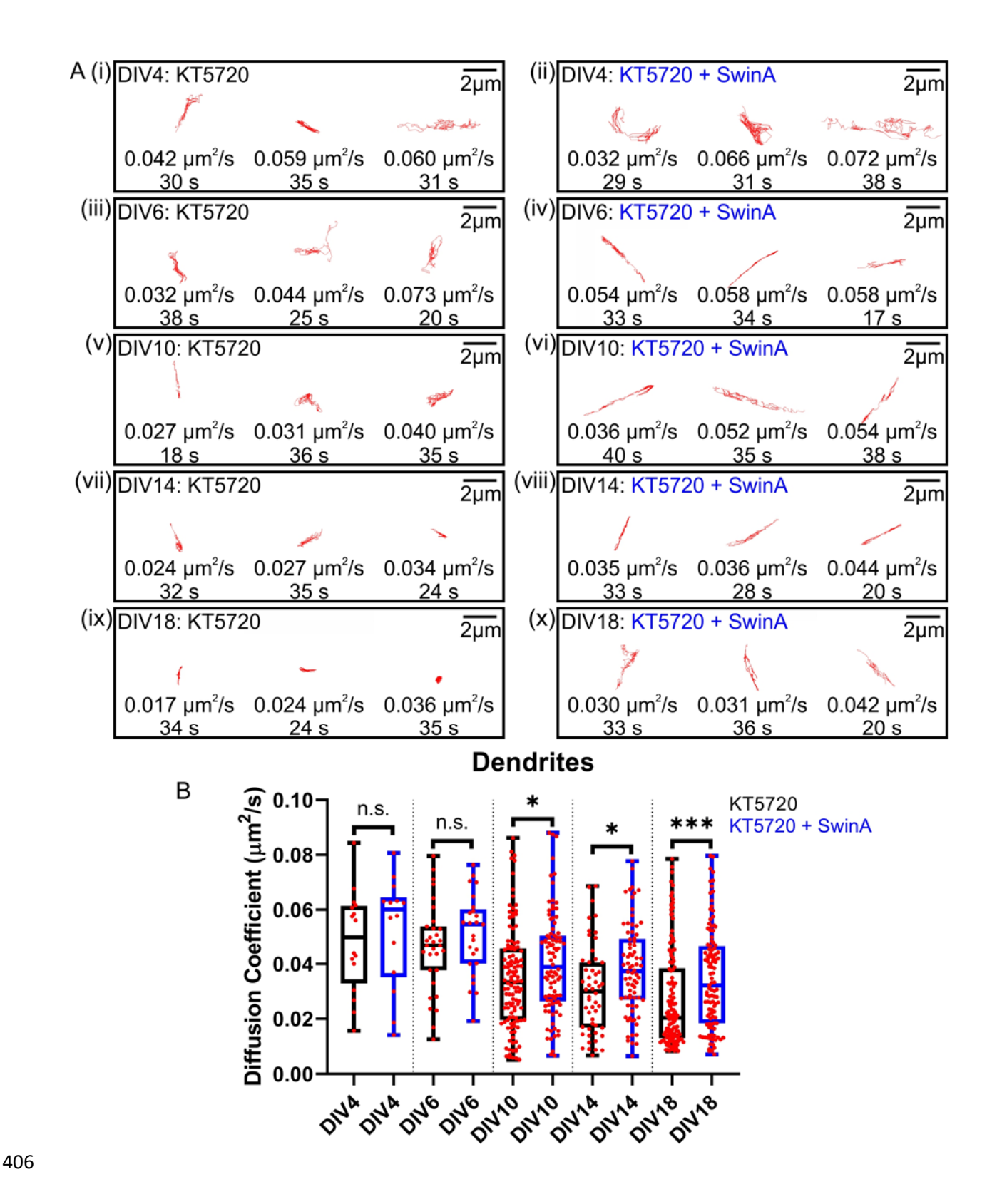


Fig. 5. Diffusion of SK channels in the plasma membrane of dendrites. (A) Representative diffusion trajectories of SK channels in the plasma membrane of dendrites at various

developmental time points after a 30-min preincubation with 1 µM KT5720 or 1 µM KT5720 409 followed by a 30-min incubation with 125 nM SwinA. (B) Box and whisker plots showing the 410 diffusion coefficients of SK channels on dendrites under different conditions at various 411 developmental time points: DIV4 (KT5720: $D = 0.048 \pm 0.019 \,\mu m^2 / s$, n = 16; KT5720 + 412 SwinA: $D = 0.053 \pm 0.020 \,\mu m^2 / s$, n = 14), DIV6 (KT5720: $D = 0.046 \pm 0.016 \,\mu m^2 / s$, 413 n = 31; KT5720 + SwinA: $D = 0.051 \pm 0.015 \,\mu m^2 / s$, n = 25), DIV10 (KT5720: D =414 $0.034 \pm 0.019 \,\mu m^2 / s$, n = 121; KT5720 + SwinA: $D = 0.040 \pm 0.019 \,\mu m^2 / s$, n = 92), 415 DIV14 (KT5720: $D = 0.031 \pm 0.016 \,\mu\text{m}^2 / \text{s}$, n = 52; KT5720 + SwinA: $D = 0.038 \pm 0.016 \,\mu\text{m}^2 / \text{s}$ 416 $0.017 \ \mu m^2 / s$, n = 76), and DIV18 (KT5720: $D = 0.027 \pm 0.018 \ \mu m^2 / s$, n = 125; KT5720 417 + SwinA: $D = 0.035 \pm 0.019 \,\mu m^2 / s$, n = 111). n.s., no significant difference. *** P < 0.001, 418 * P < 0.05 (Mann–Whitney test). 419

420

Finally, we assessed the diffusion of SK channels in the AIS. To distinguish an AIS from dendrites, 421 we imaged Alexa Fluor 568 fluorophores bound to NF186 antibodies, which is specific to AIS ¹⁰. 422 At DIV4, we observed diffusion of SK channels in the AIS in the control group, with no significant 423 increase in the SK channel diffusion coefficient following treatment with SwinA [Fig. 6A(i), A(ii), 424 B; DIV4 (KT5720): $D = 0.044 \pm 0.018 \,\mu m^2 / s$; DIV4 (KT5720 + SwinA): $D = 0.045 \pm 0.018 \,\mu m^2 / s$ 425 $0.021 \,\mu m^2 / s$, P > 0.9999]. Strikingly, most of the SK channels in the AIS became totally 426 immobile at DIV6, which was prevented by treating neurons with SwinA [Fig. 6A(iii), A(iv), B; 427 DIV6 (KT5720): $D = 0.005 \pm 0.002 \,\mu m^2 / s$; DIV6 (KT5720 + SwinA): $D = 0.022 \pm 0.002 \,\mu m^2 / s$ 428 $0.019 \,\mu m^2 / s$, P = 0.0072]. Studies have reported that the actin-associated periodic skeleton is 429 formed by DIV5 in the AIS 8,33. Our results suggest that the actin-based cytoskeleton introduces 430

diffusion barriers that restrict SK channel diffusion, and that SwinA-induced disruption of the 431 cytoskeleton increases SK channel mobility. 432 433 At DIV10, we observed no diffusion of SK channels in the AIS in the control group. However, treating neurons with SwinA mobilized the SK channels at the AIS [Fig. 6A(v), A(vi), B; DIV10 434 (KT5720): $D = 0.004 \pm 0.002 \,\mu m^2 / s$; DIV10 (KT5720 + SwinA): $D = 0.015 \pm 0.010 \,\mu m^2 / s$ 435 s, P = 0.0281]. Finally, we found that all SK channels were trapped in the AIS independent of 436 the presence of SwinA at DIV14 [Fig. 6A(vii), A(viii), B; DIV14 (KT5720): $D = 0.002 \pm 0.002$ 437 $0.001 \,\mu m^2 / s$; DIV14 (KT5720 + SwinA): $D = 0.003 \pm 0.001 \,\mu m^2 / s$, P = 0.8329] and 438 DIV18 [Fig. 6A(ix), A(x), B; DIV18 (KT5720): $D = 0.002 \pm 0.001 \,\mu m^2 / s$; DIV18 (KT5720 + 439 SwinA): $D = 0.002 \pm 0.002 \,\mu m^2 / s$, P = 0.8868]. This result indicates that as neurons reach 440 maturation at DIV14, the high density of membrane proteins generates a crowding effect that fully 441 immobilizes SK channels at the AIS plasma membrane even with disruption of the actin-based 442 membrane skeleton. Overall, we conjecture that actin-based membrane skeleton barriers are 443 444 already established in the AIS by DIV6. After neurons mature, the proteins anchored by this barrier

form a strong crowding effect that greatly restricts SK channel diffusion.

445

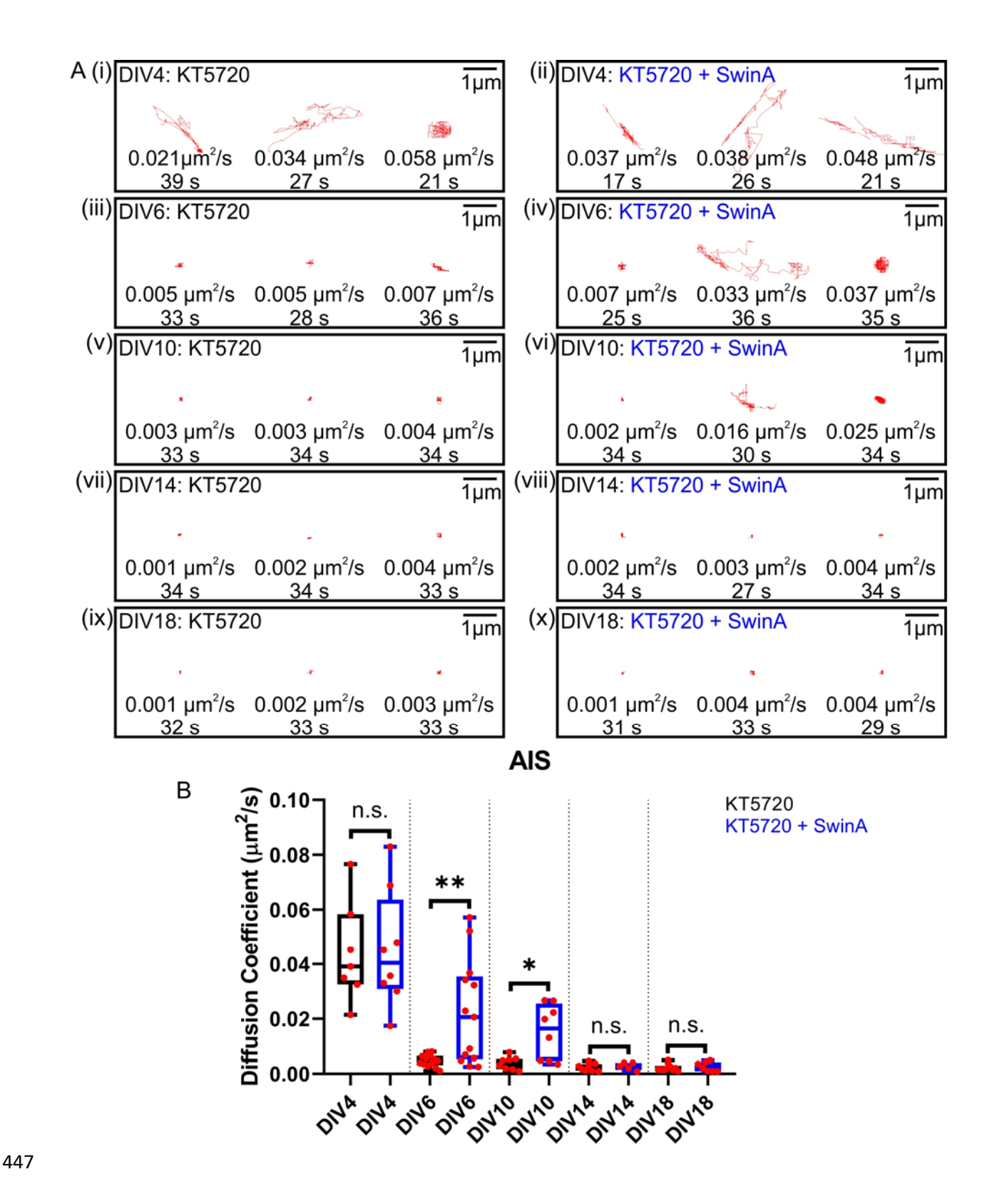


Fig. 6. Diffusion of SK channels in the plasma membrane of the AIS. (A) Representative diffusion trajectories of SK channels on the AIS at various developmental time after a 30-min

preincubation with 1 µM KT5720 or 1 µM KT5720 followed by a 30-min incubation with 125 nM 450 SwinA. (B) Box and whisker plots showing the diffusion coefficients of SK channels on the AIS 451 452 under different conditions at various developmental time points: DIV4 (KT5720: $D = 0.044 \pm$ $0.018 \,\mu m^2 / s$, n = 7; KT5720 + SwinA: $D = 0.045 \pm 0.021 \,\mu m^2 / s$, n = 8), DIV6 453 $(KT5720: D = 0.005 \pm 0.002 \,\mu m^2 / s, n = 13; KT5720 + SwinA: D = 0.022 \pm 0.019 \,\mu m^2 / s)$ 454 s, n = 13), DIV10 (KT5720: $D = 0.004 \pm 0.002 \,\mu m^2 / s$, n = 8; KT5720 + SwinA: $D = 0.004 \pm 0.002 \,\mu m^2 / s$ 455 $0.015 \pm 0.010 \,\mu m^2 / s$, n = 8), DIV14 (KT5720: $D = 0.002 \pm 0.001 \,\mu m^2 / s$, n = 8; 456 KT5720 + SwinA: $D = 0.003 \pm 0.001 \,\mu m^2 / s$, n = 5), and DIV18 (KT5720: $D = 0.002 \pm 0.001 \,\mu m^2 / s$ 457 $0.001 \,\mu m^2 / s$, n = 10; KT5720 + SwinA: $D = 0.002 \pm 0.002 \,\mu m^2 / s$, n = 7). n.s., no 458 significant difference. ** P < 0.01, * P < 0.05 (Mann–Whitney test). 459 We finally performed additional experiments to validate that our SPT method can indeed 460 distinguish between different membrane viscosities. Specifically, at DIV4 we added 1.5 mL of 461 1.5mM, 3mM, and 5mM MβCD-cholesterol complex solutions to neuron cultures. Then, in order 462 to confirm that cholesterol levels were increased after incubation with MBCD-cholesterol solution 463 in all neuronal compartments, we used filipin, which specifically stains cholesterol, following the 464 465 protocol described in methods. We indeed observed a significant increase in corrected total fluorescence (CTF) ratio of the filipin-conjugated cholesterol in all cases compared to control (Fig. 466 S4 A,B,C). We also detected a significant difference between control samples and neurons 467 468 incubated in 1.5mM MβCD-cholesterol solution but not a significant difference between neuron samples incubated in 3mM and 5mM MβCD-cholesterol solutions. 469

26

470

After confirming that incubation with M β CD-cholesterol resulted in an increase of cholesterol, we performed SPT experiments on live neurons. We observed a significant decrease in the diffusion coefficients of QD-conjugated SK channels in all neuronal compartments in the cases of 3mM and 5mM, for which we measured SK diffusion coefficients less than $0.02 \, \mu m^2 / s$, compared to control cases, for which we measured SK diffusion coefficients close to $0.04 \, \mu m^2 / s$. However, we were not able to detect a difference between control samples and neurons incubated in 1.5mM M β CD-cholesterol solution and between neuron samples incubated in 3mM and 5mM M β CD-cholesterol solutions. Overall, we confirmed that our technic has the resolution to measure differences in SK diffusion coefficients on the order of $0.02 \, \mu m^2 / s$, which is the difference levels measured in neurons during development and when the actin network was disorganized using SwinA and CytoD.

Discussion

In this study, we employed SPT to study the diffusion of streptavidin-conjugated QDs labeling apamin-biotin-tagged SK channels by using TIRF microscopy in HEK293T cells and in different neuronal compartments for various neuronal development time points. Recent work has shown that QDs can potentially affect the lateral diffusion and transition state of target receptors ³⁴. Nevertheless, our results based on QD tracking still provided substantial information regarding both dynamic changes in SK channel diffusion and the impact of the actin-based membrane skeleton on SK diffusion. QDs are well known for their stable and bright fluorescence compared with traditional fluorophores ³⁵; therefore, QDs perfectly matched our requirements for long-term evaluation of SK channel diffusion, even though they might weaken SK channel mobility. Our results highlight the effect of actin filaments in reducing the mobility of SK channels.

The SK channel diffusion trajectories obtained in the soma [Fig. 4A(i), 4A(iii), 4A(v), 4A(vii), 4A(ix)] indicate the gradual formation of a 2D actin-based skeleton lattice, which caused a decrease in the diffusion coefficients DIV10, 14, and 18 (Fig. 4B). In support of this finding, the addition of SwinA, which degrades the actin cytoskeleton, resulted in larger QD trajectories and higher diffusion coefficients than those observed for the untreated cases at DIV10, 14, and 18, when the actin cytoskeleton is expected to be more developed than that for the earlier time points of DIV4 and 6 [Fig. 4A(ii), 4A(iv), 4A(vi), 4A(viii), 4A(x), 4B]. This result is in agreement with previous findings ^{32,36}. We also note that the observed significant linear trend of diffusion coefficient decrease from DIV4 to DIV10 and subsequent diffusion coefficient stability from DIV10 to DIV18, in both control and SwinA-treated groups, is in agreement with a gradual formation of the membrane skeleton in somasuntil DIV10; and minimal or no development of the membrane skeleton after DIV10. Our data are also compatible with the finding that treatment with SwinA causes a significant increase in diffusion in DIV10, 14, and 18 but no significant change in DIV4 and 6. This is because disruption of a well-formed membrane skeleton would have a more substantial effect on diffusion than disruption of a membrane skeleton still under development. Measurements in dendrites are similar to those observed in the soma. As neurons mature and the actin cytoskeleton becomes more developed, the diffusion trajectories become shorter [Fig. 5A(i), 5A(iii), 5A(v), 5A(vii), 5A(ix)], and the diffusion coefficients are lower at DIV10, 14, and 18. Again, the addition of SwinA resulted in larger diffusion trajectories and higher diffusion coefficients at DIV10, 14, and 18 [Fig. 5A(vi), 5A(viii), 5A(x), 5B]. The restriction was a gradual process in the somatodendritic regions, whereas at the AIS, SK channels were totally immobile by DIV6. However, previous work has shown that the actin and spectrin periodic rings are already formed at the AIS at DIV2 33,37. Our results showed that SK

495

496

497

498

499

500

501

502

503

504

505

506

507

508

509

510

511

512

513

514

515

516

channels were still mobile at the AIS at DIV4, leading to the question of why SK channel diffusion was not restricted since actin-based diffusion barriers had already been established. We considered four possible explanations that could reconcile these observations. First, although actin-staining results showed a periodic pattern at DIV2 33,37, the actin might exist as short segments instead of a complete assembly. Supporting this conjecture, studies have shown that adducin, which stabilizes actin filaments and promotes the formation of the actin-spectrin network, starts to exhibit periodicity in the AIS at DIV6 rather than DIV2 37,38. This finding indicates that the actin–spectrin periodic network found at DIV2 might not have been fully formed, allowing for greater SK channel diffusion. Second, it is true that at DIV2 live imaging of the AIS by harnessing the Sir-actin probe, which is based on the toxin Jasplakinolide, exhibited the actin periodic strip structure ³⁹. However, Jasplakinolide has been previously reported to promote actin polymerization and stabilization ⁴⁰. Third, due to differences in neuron cultures, our neurons might develop more slowly, which may have caused a delay in actin–spectrin network formation at the AIS. Fourth, it is also possible that not all SK channels interact with the actin cytoskeleton earlier in development. Importantly, when we applied the actin disruption drug SwinA, the SK channels were almost immobile at DIV14 and 18 instead of DIV6 and 10, with SwinA application resulting in increased SK mobility. We speculate that after DIV14, membrane proteins concentrated and anchored at the AIS likely generated a crowding effect, which may have contributed to the immobilization of SK channels. In support of this hypothesis, a study reported that AnkG proteins assemble into a periodic cytoskeleton by DIV12 37 and thus their binding partners (e.g., NF186, neuronal cell adhesion molecule (NrCAM), and Nav channels) are also immobilized in the plasma membrane after DIV12, contributing to the crowding effect.

518

519

520

521

522

523

524

525

526

527

528

529

530

531

532

533

534

535

536

537

538

Moreover, neurofascin and NrCAM almost reach their maximum recruitment at the AIS by 14 and DIV10, respectively 41. The accumulation of Nav channels occurs by DIV12 at the AIS 42. In addition, by DIV12, β2-spectrin subunits are replaced by β4-spectrin subunits in the AIS ³⁷. Researchers have suggested that L1 cell adhesion molecule 43 and Nav channels are associated with β4-spectrin ⁴⁴. The other end of AnkG is connected to microtubules through microtubuleassociated proteins such as Ndel1, EB1, and EB3 45,46. In particular, previous work has shown that the percentage of neurons with EB3 concentrated at the AIS increases from approximately 22% at DIV7 to approximately 70% at DIV14 45. Together, these results suggest that by DIV14, AnkG proteins were assembled in the periodic cytoskeleton of the AIS and anchored massive AISspecific proteins in the plasma membrane, generating a crowding effect that greatly inhibited SK channel diffusion. In addition, the actin-based membrane skeleton is connected to microtubules via AnkG and other proteins at this time point, which makes the entire assembly even more robust. We finally note that experiments by Vassilopoulos et al. ⁴⁷ showed that application of SwinA to DIV13-17 neurons partially disrupted periodic arrangements of actin rings in the AIS without a significant effect on the periodicity of β 4-spectrin. It is not clear if the observed robustness of the periodic distribution of \beta4-spectrin compared to actin was exclusively due to crowding or if attachment of \beta4-spectrin to actin and to AnkG played a role as well. Based on the aforementioned reasoning, we are unsure whether the mechanisms underlying the behavior of β4-spectrin and SK channels in mature neurons treated with SwinA are similar.

559

560

561

562

540

541

542

543

544

545

546

547

548

549

550

551

552

553

554

555

556

557

558

In conclusion, we employed SPT to study the diffusion of streptavidin-QDs labeling apamin-biotin-tagged SK channels via TIRF microscopy. We examined the diffusion of SK channels in HEK293T cells and different neuronal compartments at various neuronal development time points.

Our results show that as neurons mature, the membrane skeleton becomes more actin-based, which 563 impedes the diffusion of SK channels. In addition, the crowding effect in the plasma membrane of 564 the AIS also contributes to the immobilization of SK channels in mature neurons. 565 566 Acknowledgments 567 This work was supported by the National Science Foundation Division of Physics, Physics of 568 Living Systems 2210535 and by the Division of Civil, Mechanical and Manufacturing Innovation 569 570 Career Award 1351363 to G. Lykotrafitis. **Conflicts of interest** 571 The authors declare no conflicts of interest. 572 **Author Contributions** 573 S. Gu, A.V. Tzingounis, and G. Lykotrafitis designed the research; S. Gu conducted the research 574 and collected the data; S. Gu, A.V. Tzingounis, and G. Lykotrafitis analyzed and interpreted the 575 576 data; A.V. Tzingounis and G. Lykotrafitis contributed new reagents and analytic tools; S. Gu, A.V. Tzingounis, and G. Lykotrafitis wrote the paper. 577 **Data Availability** 578 The data underlying this article will be shared on reasonable request to the corresponding author. 579 580 581 582 583

References:

586

- 1. Lin MT, Lujan R, Watanabe M, Adelman JP, Maylie J. SK2 channel plasticity contributes to LTP at Schaffer collateral-CA1 synapses. *Nat Neurosci.* 2008;11 (2):170-177. doi: 10.1038/nn2041.
- 2. Ren Y, Barnwell LF, Alexander JC, et al. Regulation of surface localization of the small conductance Ca2+-activated potassium channel, Sk2, through direct phosphorylation by cAMP-dependent protein kinase. *J Biol Chem.* 2006;281 (17):11769-11779. doi: 10.1074/jbc.M513125200.
- Faber ES, Sah P. Functions of SK channels in central neurons. *Clin Exp Pharmacol Physiol.* 2007;34 (10):1077-1083. doi: 10.1111/j.1440-1681.2007.04725.x.
- Abiraman K, Sah M, Walikonis RS, Lykotrafitis G, Tzingounis AV. Tonic PKA Activity Regulates SK
 Channel Nanoclustering and Somatodendritic Distribution. *J Mol Biol.* 2016;428 (11):2521-2537.
 doi: 10.1016/j.jmb.2016.04.014.
- 598 5. Zhang Z, Ledford HA, Park S, et al. Distinct subcellular mechanisms for the enhancement of the
 599 surface membrane expression of SK2 channel by its interacting proteins, α-actinin2 and filamin
 600 A. The Journal of physiology. 2017;595 (7):2271-2284. doi: 10.1113/jp272942.
- 6. Lu L, Zhang Q, Timofeyev V, et al. Molecular coupling of a Ca2+-activated K+ channel to L-type 602 Ca2+ channels via alpha-actinin2. *Circulation research*. 2007;100 (1):112-120. doi: 603 10.1161/01.res.0000253095.44186.72.
- Lu L, Timofeyev V, Li N, et al. Alpha-actinin2 cytoskeletal protein is required for the functional
 membrane localization of a Ca2+-activated K+ channel (SK2 channel). *Proc Natl Acad Sci U S A*.
 2009;106 (43):18402-18407. doi: 10.1073/pnas.0908207106.
- 8. Xu K, Zhong G, Zhuang X. Actin, spectrin, and associated proteins form a periodic cytoskeletal structure in axons. *Science*. 2013;339 (6118):452-456. doi: 10.1126/science.1232251.
- 509 9. Zhang Y, Tzingounis AV, Lykotrafitis G. Modeling of the axon plasma membrane structure and its
 610 effects on protein diffusion. *PLoS Comput Biol.* 2019;15 (5):e1007003. doi:
 611 10.1371/journal.pcbi.1007003.
- 612 10. Albrecht D, Winterflood CM, Sadeghi M, Tschager T, Noe F, Ewers H. Nanoscopic 613 compartmentalization of membrane protein motion at the axon initial segment. *J Cell Biol.* 614 2016;215 (1):37-46. doi: 10.1083/jcb.201603108.
- Borgdorff AJ, Choquet D. Regulation of AMPA receptor lateral movements. *Nature*. 2002;417 (6889):649-653. doi: 10.1038/nature00780.
- 617 12. Messier C, Mourre C, Bontempi B, Sif J, Lazdunski M, Destrade C. Effect of apamin, a toxin that inhibits Ca(2+)-dependent K+ channels, on learning and memory processes. *Brain Res.* 1991;551 (1-2):322-326. doi: 10.1016/0006-8993(91)90950-z.
- Voos P, Yazar M, Lautenschlager R, Rauh O, Moroni A, Thiel G. The small neurotoxin apamin
 blocks not only small conductance Ca(2+) activated K(+) channels (SK type) but also the voltage
 dependent Kv1.3 channel. Eur Biophys J. 2017;46 (6):517-523. doi: 10.1007/s00249-016-1196-0.
- Ishii TM, Maylie J, Adelman JP. Determinants of apamin and d-tubocurarine block in SK
 potassium channels. *J Biol Chem.* 1997;272 (37):23195-23200. doi: 10.1074/jbc.272.37.23195.
- Abiraman K, Tzingounis AV, Lykotrafitis G. KCa2 channel localization and regulation in the axon initial segment. *FASEB J.* 2018;32 (4):1794-1805. doi: 10.1096/fj.201700605R.
- Hochbaum DR, Zhao Y, Farhi SL, et al. All-optical electrophysiology in mammalian neurons using engineered microbial rhodopsins. *Nat Methods*. 2014;11 (8):825-833. doi: 10.1038/nmeth.3000.
- Jaqaman K, Loerke D, Mettlen M, et al. Robust single-particle tracking in live-cell time-lapse
 sequences. *Nat Methods*. 2008;5 (8):695-702. doi: 10.1038/nmeth.1237.

- Faber ES, Delaney AJ, Power JM, Sedlak PL, Crane JW, Sah P. Modulation of SK channel trafficking by beta adrenoceptors enhances excitatory synaptic transmission and plasticity in the amygdala. *J Neurosci.* 2008;28 (43):10803-10813. doi: 10.1523/jneurosci.1796-08.2008.
- Maciaszek JL, Soh H, Walikonis RS, Tzingounis AV, Lykotrafitis G. Topography of native SK
 channels revealed by force nanoscopy in living neurons. *J Neurosci.* 2012;32 (33):11435-11440.
 doi: 10.1523/JNEUROSCI.1785-12.2012.
- Tamkun MM, O'Connell K M, Rolig AS. A cytoskeletal-based perimeter fence selectively corrals a sub-population of cell surface Kv2.1 channels. *J Cell Sci.* 2007;120 (Pt 14):2413-2423. doi: 10.1242/jcs.007351.
- Vasilev F, Ezhova Y, Chun JT. Signaling Enzymes and Ion Channels Being Modulated by the Actin Cytoskeleton at the Plasma Membrane. *International journal of molecular sciences*. 2021;22 (19). doi: 10.3390/ijms221910366.
- Venkatesh K, Mathew A, Koushika SP. Role of actin in organelle trafficking in neurons. *Cytoskeleton (Hoboken, NJ).* 2020;77 (3-4):97-109. doi: 10.1002/cm.21580.
- Bubb MR, Spector I, Bershadsky AD, Korn ED. Swinholide A is a microfilament disrupting marine toxin that stabilizes actin dimers and severs actin filaments. *J Biol Chem.* 1995;270 (8):3463-3466. doi: 10.1074/jbc.270.8.3463.
- Gil-Krzewska A, Saeed MB, Oszmiana A, et al. An actin cytoskeletal barrier inhibits lytic granule
 release from natural killer cells in patients with Chediak-Higashi syndrome. *The Journal of allergy* and clinical immunology. 2018;142 (3):914-927.e916. doi: 10.1016/j.jaci.2017.10.040.
- Gibbon BC, Kovar DR, Staiger CJ. Latrunculin B has different effects on pollen germination and tube growth. *Plant Cell.* 1999;11 (12):2349-2363. doi: 10.1105/tpc.11.12.2349.
- Spector I, Shochet NR, Kashman Y, Groweiss A. Latrunculins: novel marine toxins that disrupt microfilament organization in cultured cells. *Science*. 1983;219 (4584):493-495. doi: 10.1126/science.6681676.
- Cooper JA. Effects of cytochalasin and phalloidin on actin. *J Cell Biol.* 1987;105 (4):1473-1478.
 doi: 10.1083/jcb.105.4.1473.
- Schliwa M. Action of cytochalasin D on cytoskeletal networks. *J Cell Biol.* 1982;92 (1):79-91. doi: 10.1083/jcb.92.1.79.
- Rubtsova SN, Kondratov RV, Kopnin PB, Chumakov PM, Kopnin BP, Vasiliev JM. Disruption of actin microfilaments by cytochalasin D leads to activation of p53. *FEBS Letters*. 1998;430 (3):353-357. doi: https://doi.org/10.1016/S0014-5793(98)00692-9.
- 663 30. Leterrier C, Potier J, Caillol G, Debarnot C, Rueda Boroni F, Dargent B. Nanoscale Architecture of 664 the Axon Initial Segment Reveals an Organized and Robust Scaffold. *Cell Rep.* 2015;13 (12):2781-665 2793. doi: 10.1016/j.celrep.2015.11.051.
- Abouelezz A, Micinski D, Lipponen A, Hotulainen P. Sub-membranous actin rings in the axon initial segment are resistant to the action of latrunculin. *Biological chemistry*. 2019;400 (9):1141-1146. doi: 10.1515/hsz-2019-0111.
- Han B, Zhou R, Xia C, Zhuang X. Structural organization of the actin-spectrin-based membrane
 skeleton in dendrites and soma of neurons. *Proc Natl Acad Sci U S A.* 2017;114 (32):E6678 E6685. doi: 10.1073/pnas.1705043114.
- 672 33. D'Este E, Kamin D, Gottfert F, El-Hady A, Hell SW. STED nanoscopy reveals the ubiquity of 673 subcortical cytoskeleton periodicity in living neurons. *Cell Rep.* 2015;10 (8):1246-1251. doi: 674 10.1016/j.celrep.2015.02.007.
- Abraham L, Lu HY, Falcao RC, et al. Limitations of Qdot labelling compared to directlyconjugated probes for single particle tracking of B cell receptor mobility. *Sci Rep.* 2017;7 (1):11379. doi: 10.1038/s41598-017-11563-9.

- Garcia de Arquer FP, Talapin DV, Klimov VI, Arakawa Y, Bayer M, Sargent EH. Semiconductor quantum dots: Technological progress and future challenges. *Science*. 2021;373 (6555). doi: 10.1126/science.aaz8541.
- Sadegh S, Higgins JL, Mannion PC, Tamkun MM, Krapf D. Plasma Membrane is
 Compartmentalized by a Self-Similar Cortical Actin Meshwork. *Phys Rev X*. 2017;7 (1). doi:
 10.1103/PhysRevX.7.011031.
- Zhong G, He J, Zhou R, et al. Developmental mechanism of the periodic membrane skeleton in axons. *Elife*. 2014;3. doi: 10.7554/eLife.04581.
- Kiang KM, Leung GK. A Review on Adducin from Functional to Pathological Mechanisms: Future Direction in Cancer. *Biomed Res Int.* 2018;2018:3465929. doi: 10.1155/2018/3465929.
- Lukinavicius G, Reymond L, D'Este E, et al. Fluorogenic probes for live-cell imaging of the cytoskeleton. *Nat Methods*. 2014;11 (7):731-733. doi: 10.1038/nmeth.2972.
- 40. Holzinger A. Jasplakinolide: an actin-specific reagent that promotes actin polymerization.
 691 *Methods Mol Biol.* 2009;586:71-87. doi: 10.1007/978-1-60761-376-3 4.
- Jones SL, Korobova F, Svitkina T. Axon initial segment cytoskeleton comprises a multiprotein
 submembranous coat containing sparse actin filaments. *J Cell Biol.* 2014;205 (1):67-81. doi:
 10.1083/jcb.201401045.
- Nakada C, Ritchie K, Oba Y, et al. Accumulation of anchored proteins forms membrane diffusion barriers during neuronal polarization. *Nat Cell Biol.* 2003;5 (7):626-632. doi: 10.1038/ncb1009.
- 43. Nishimura K, Akiyama H, Komada M, Kamiguchi H. betaIV-spectrin forms a diffusion barrier
 698 against L1CAM at the axon initial segment. *Mol Cell Neurosci.* 2007;34 (3):422-430. doi:
 10.1016/j.mcn.2006.11.017.
- 700 44. Nip K, Kashiwagura S, Kim JH. Loss of beta4-spectrin impairs Nav channel clustering at the 701 heminode and temporal fidelity of presynaptic spikes in developing auditory brain. *Sci Rep.* 702 2022;12 (1):5854. doi: 10.1038/s41598-022-09856-9.
- 45. Leterrier C, Vacher H, Fache MP, et al. End-binding proteins EB3 and EB1 link microtubules to
 704 ankyrin G in the axon initial segment. *Proc Natl Acad Sci U S A.* 2011;108 (21):8826-8831. doi:
 705 10.1073/pnas.1018671108.
- Kuijpers M, van de Willige D, Freal A, et al. Dynein Regulator NDEL1 Controls Polarized Cargo
 Transport at the Axon Initial Segment. *Neuron.* 2016;89 (3):461-471. doi:
 10.1016/j.neuron.2016.01.022.
- Vassilopoulos S, Gibaud S, Jimenez A, Caillol G, Leterrier C. Ultrastructure of the axonal periodic
 scaffold reveals a braid-like organization of actin rings. *Nature Communications*. 2019;10
 (1):5803. doi: 10.1038/s41467-019-13835-6.